Available online at www.sciencedirect.com
ScienceDirect
International Journal of Thermal Sciences 46 (2007) 57–66
International Journal of Thermal Sciences
www.elsevier.com/locate/ijts

Experimental microchannel heat sink performance studies using nanofluids

Reiyu Chein *, Jason Chuang

Department of Mechanical Engineering, National Chung Hsing University, 250 Kuo-Kuang Rd., Taichung City, Taiwan 402

Received 4 October 2005; received in revised form 24 February 2006; accepted 3 March 2006

Available online 6 June 2006

Abstract

In this study, microchannel heat sink (MCHS) performance using nanofluids as coolants is addressed. We first carried out a simple theoretical analysis that indicated more energy and lower MCHS wall temperature could be obtained under the assumption that heat transfer could be enhanced by the presence of nanoparticles. Experiments were then performed to verify the theoretical predictions. A silicon MCHS was made and CuO–H_2O mixtures without a dispersion agent were used as the coolants. The CuO particle volume fraction was in the range of 0.2 to 0.4%. It was found that nanofluid-cooled MCHS could absorb more energy than water-cooled MCHS when the flow rate was low. For high flow rates, the heat transfer was dominated by the volume flow rate and nanoparticles did not contribute to the extra heat absorption. The measured MCHS wall temperature variations agreed with the theoretical prediction for low flow rate. For high flow rate, the measured MCHS wall temperatures did not completely agree with the theoretical prediction due to the particle agglomeration and deposition. It was also found that raising the nanofluid bulk temperature could prevent the particles from being agglomerated into larger scale particle clusters. The experimental result also indicated that only slightly increase in pressure drop due to the presence of nanoparticles in MCHS operation.
© 2006 Elsevier Masson SAS. All rights reserved.

Keywords: Microchannel heat sink (MCHS); Nanofluid; Particle volume fraction and particle agglomeration

1. Introduction

Since the pioneer work by Tuckerman and Pease [1], the microchannel heat sink (MCHS) has received extensive study over the past two decades because of its capability to dissipate large amounts of heat from a small area. A MCHS typically contains a large number of parallel microchannels with a hydraulic diameter ranging from 10 to 1000 μm. Coolant is forced to pass through these channels to carry heat away from a hot surface. Experimental studies have shown that the MCHS has several distinct features compared to conventional heat dissipating devices, i.e., the ability to produce a very high heat transfer coefficient, very small size and volume per heat load, and small coolant requirements [2,3]. In addition to experimental studies, heat transfer predictions and geometry optimizations based on theoretical analysis and numerical modeling were carried out extensively in previous investigations [4,5].

The most frequently used coolants in the MCHS study were air, water, and fluoro-chemicals. The heat transfer capability is limited by the working fluid transport properties. One of the methods for enhancing heat transfer is the application of additives to the working fluids. The basic idea is to enhance the heat transfer by changing the fluid transport properties and flow features [6,7]. Recent interest based on this concept focused on heat transfer enhancement using a nanofluid in which nanoscale metallic or nonmetallic particles are suspended in the base fluids. The experimental and analytical studies by Wang et al. [8], Lee et al. [9], Wang et al. [10], and Koo and Kleinstreuer [11] showed that nanofluids have higher thermal conductivity than pure fluids and therefore great potential for heat transfer enhancement.

There have been relatively few studies on nanofluid flow and heat transfer characteristics comparing with studies on pure fluids. Xuan and Roetzel [12] proposed two theoretical models to predict the heat transfer characteristics in a nanofluid tube flow. Li and Xuan [13], Xuan and Li [14] and Pak and Cho [15] experimentally measured the convection heat trans-

* Corresponding author. Tel.: +886 4 22850462; fax: +886 4 22877170.
E-mail address: rychein@dragon.nchu.edu.tw (R. Chein).

1290-0729/$ – see front matter © 2006 Elsevier Masson SAS. All rights reserved.
doi:10.1016/j.ijthermalsci.2006.03.009

Nomenclature

C_p	specific heat	$J\,kg^{-1}\,K^{-1}$	
H	depth of the microchannel	m	
h	local heat transfer coefficient	$W\,m^{-2}\,K^{-1}$	
k	thermal conductivity	$W\,m^{-1}\,K^{-1}$	
Q	heating rate absorbed by working fluid	W	
Q_{in}	total heating power	W	
q''	heat flux	$W\,m^{-2}$	
T_s	microchannel inner wall temperature	K	
$T_{s\,max}$	maximum microchannel inner wall temperature	K	
T_i	coolant inlet temperature	K	
T_o	coolant outlet temperature	K	
R_{th}	heat sink thermal resistance	$°C\,W^{-1}$	
SH	particle shape factor		
$\dot{V}$	coolant volumetric flow rate	$mL\,min^{-1}$	
W_{ch}	width of microchannel	m	
W_{fin}	width of microchannel wall	m	
W_b	bottom width of the microchannel	m	
W_f	width of the microchannel wall	m	
W_t	top width of the microchannel	m	
XI	locations at the MCHS base plate for temperature measurement, $I = 1, 2, 3$		

Greek symbols

μ	viscosity	$kg\,m^{-1}\,s^{-1}$
ρ	density	$kg\,m^{-3}$
ϕ	particle volume fraction	%

Subscript

f	pure fluid
nf	nanofluid
p	particle

fer and pressure drop for nanofluid tube flows. Their results indicated that the heat transfer coefficient was greatly enhanced and depended on the Reynolds flow number, particle Peclet number, the particle size and shape, and particle volume fraction. They also found that nanoparticles did not cause an extra pressure drop. Recently, Yang et al. [16] carried out an experimental study attempting to construct a heat transfer correlation among the parameters that affected heat transfer. For a laminar flow regime in a circular tube, they indicated that the heat transfer coefficient for the nanofluid flow has a lower increase than predicted by either the conventional heat transfer correlation for the homogeneous or particle-suspended fluid.

In most of the studies mentioned above, the heat transfer characteristics of nanofluid flow were carried out in macroscale dimensions. The study of heat transfer characteristics in the microscale dimension needs further exploration. Koo and Kleinstreuer [17] reported a theoretical investigation on the MCHS using a nanofluid as the coolant. Chein and Huang [18] employed the macroscale correlation to predict the microchannel heat sink performance. To our best knowledge, no experimental data were reported on the microchannel heat sink using a nanofluid as the coolant. In this study, we focus on the effects of nanoparticle concentration and nanofluid flow rate on the performance of MCHS. Microchannel size is also one of the factors that affecting the nanofluid-cooled MCHS performance. For reducing the number of factors that affecting the heat transfer using nanofluid, MCHS with one fixed microchannel dimension is investigated. A simple prediction of the heat transfer characteristics in MCHS using a nanofluid was first examined. The conclusions for the theoretical predictions were then verified using experimental studies. Detailed comparisons between the pure fluid- and nanofluid-cooled MCHS performances were discussed. Factors that affected the temperature measurements, such as nanoparticle agglomeration and deposition were also examined.

2. Theoretical prediction

A nanofluid can be considered a liquid–solid mixture in which nanoparticles are suspended in the pure fluid. Because of the presence of these particles, the thermophysical properties of the nanofluid are different from the pure fluid. The relevant properties in the heat transfer applications are the thermal conductivity, viscosity, and thermal capacity. In the literature, it can be found that these properties depend on the particle volume fraction and can be expressed as

Thermal conductivity:

$$k_{nf} = k_f \frac{k_p + (SH-1)k_f - (SH-1)\phi(k_f - k_p)}{k_p + (SH-1)k_f + \phi(k_f - k_p)} \tag{1}$$

Viscosity:

$$\mu_{nf} = \mu_f \frac{1}{(1-\phi)^{2.5}} \tag{2}$$

Thermal capacity:

$$(\rho C_p)_{nf} = (1-\phi)(\rho C_p)_f + \phi(\rho C_p)_p \tag{3}$$

Eq. (1) is regarded as the theoretical model for the nanofluid thermal conductivity proposed by Hamilton and Cross [19] based on treating nanofluid as liquid–solid mixture for static suspension. Although recent studies indicated that Eq. (1) underestimates the thermal conductivity of the nanofluid [8–11], it is usually employed as a comparison basis since fundamental factors that affecting the nanofluid thermal conductivity are included. For systems involving nanofluid flow, thermal conductivity increase due to thermal dispersion effect should be included in the evaluation of nanofluid thermal conductivity [20]. Eq. (2) is regarded as the theoretical model for the nanofluid viscosity proposed by Brinkman [21]. Recent studies also indicated that Eq. (2) underestimates the nanofluid viscosity [15]. However, the effect of the presence of particle on viscosity is clearly indicated by Eq. (2).

In the system we considered, the energy generated by the heater is absorbed either by the working fluid or by the MCHS if the heat loss to the environment is neglected. For both nanofluid- and pure fluid-cooled MCHS, energy absorbed by the working fluid can be written as,

$$Q_{nf} = (\rho C_p)_{nf} \dot{V}_{nf} (T_{nfo} - T_{nfi}) = (\rho C_p)_{nf} \dot{V}_{nf} \Delta T_{nf} \quad (4)$$

$$Q_f = (\rho C_p)_f \dot{V}_f (T_{fo} - T_{fi}) = (\rho C_p)_f \dot{V}_f \Delta T_f \quad (5)$$

Note that the thermal capacity of the nanofluid is usually smaller than that for the pure fluid because of the low specific heat of nanoparticles. According to Newton's law of cooling, the local heat transfer coefficient for both nanofluid- and pure fluid-cooled MCHS can be expressed as,

$$q'' = h_{nf}(x)\left[T_{snf}(x) - T_{nf}(x)\right] = h_f(x)\left[T_{sf}(x) - T_f(x)\right] \quad (6)$$

Using Eq. (6), we have,

$$h_{nf}(x) = \frac{q''}{T_{snf}(x) - T_{nf}(x)} \quad (7)$$

and

$$h_f(x) = \frac{q''}{T_{sf}(x) - T_f(x)} \quad (8)$$

If the nanofluid has the ability to enhance heat transfer, i.e., $h_{nf}(x) > h_f(x)$ and $Q_{nf} > Q_f$ under the conditions of $\dot{V}_{nf} = \dot{V}_f$ and $T_{nfi} = T_{fi}$, it is expected that

$$(T_{nfo} - T_{nfi}) > (T_{fo} - T_{fi}) \quad (9)$$

and

$$\left[T_{snf}(x) - T_{nf}(x)\right] < \left[T_{sf}(x) - T_f(x)\right] \quad (10)$$

Combining Eqs. (9) and (10), it can be found that

$$T_{snf}(x) < T_{sf}(x) \quad (11)$$

The result of Eq. (11) indicates that nanofluid-cooled MCHS would have lower microchannel inner wall temperature than the pure fluid-cooled MCHS. In electronic cooling applications, this implies that lower chip surface temperature can be resulted by using the nanofluid as the coolant. This can be considered as one of the benefits of employing nanofluids as coolants in the MCHS operation.

The performance of the MCHS is commonly presented by the thermal resistance defined as,

$$R_{th} = \frac{T_{s\max} - T_i}{Q_{in}} \quad (12)$$

Since the maximum wall temperature of nanofluid-cooled MCHS is lower than that of pure fluid cooled MCHS, reduction of thermal resistance in nanofluid-cooled MCHS is then expected.

Another important parameters in the MCHS operation is the pressure drop across the MCHS which relates to the coolant pumping power required. If the presence of nanoparticles in coolant did not produce extra pressure drop, it can then be considered as another benefit of using a nanofluid as the coolant in MCHS operation. In this study, the theoretical predictions stated above are to be verified experimentally. Temperature and pressure measurements at the MCHS inlet, outlet and temperature along the base plate are necessary and discussed below.

3. Experimental setup and working fluid

3.1. Experimental setup

Schematic diagram of the experimental setup is shown in Fig. 1. The main components of the test apparatus are a closed-

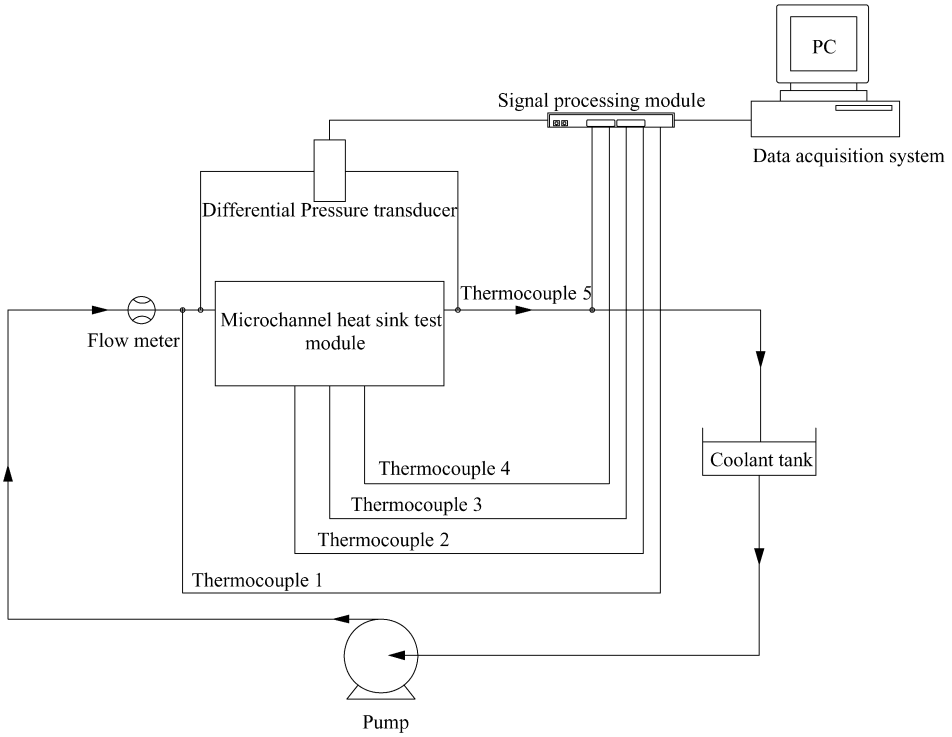

Fig. 1. Schematics of the experimental setup.

loop fluid handling system, microchannel heat sink test module and data acquisition system. In the closed-loop fluid handling system a positive-displacement pump (P151-391TI, Milton Roy, Ivyland, PA, USA) was used to provide the pressure head. It can be operated at a variable rotation speed to supply various flow rates in the loop. A differential pressure transducer along with T-type thermocouples were connected at the inlet and outlet of the microchannel test module to measure the pressure drop and temperature difference of the fluid as it flowed through the test module. A high-sensitivity flow meter (series SDN, EGE, German) was connected at the test module entrance to measure and calibrate the flow rate supplied by the pump. Before the circulated fluid entering the test module, it was dumped into a cooling device to maintain the fluid temperature at 20 °C at the test module inlet.

The microchannel heat sink test module consists of microchannel heat sink, heater, thermal insulating layer and Teflon base with a rectangular cavity. Fig. 2 shows the detail design of the microchannel heat sink used in this study. It was fabricated using standard wet etching on a 4 inch, ⟨100⟩ orientation silicon wafer. The thickness of the silicon wafer was 500 μm. A 500 μm-thick glass plate covered the top surface of the microchannels using anodic bonding to form the flow passages. Fig. 2(a) shows the cross section of a microchannel etched on the silicon wafer. The channel has a trapezoidal shape with the top width, bottom width and depth denoted as W_t, W_b, and H, respectively. W_f is the bottom width of the wall that separates the channels. The target angle between the channel sidewall and bottom wall is 54.7°. L_s is the thickness of the base plate which measured from the channel bottom wall to the base plate as shown in Fig. 2(a). Fig. 2(b) illustrates the top view of the microchannel heat sink. In addition to the parallel channels, inlet and outlet ports are also required for distributing the coolant into the microchannels and collecting coolant at the channel exits. To focus on the working fluid effect on the heat sink performance, W_t, H and W_f were fixed at 500 μm, 100 μm and 500 μm, respectively. Also shown in Fig. 2(b) are three locations at the MCHS base plate (X1, X2 and X3) where thermocouples were attached for measuring the base plate temperatures.

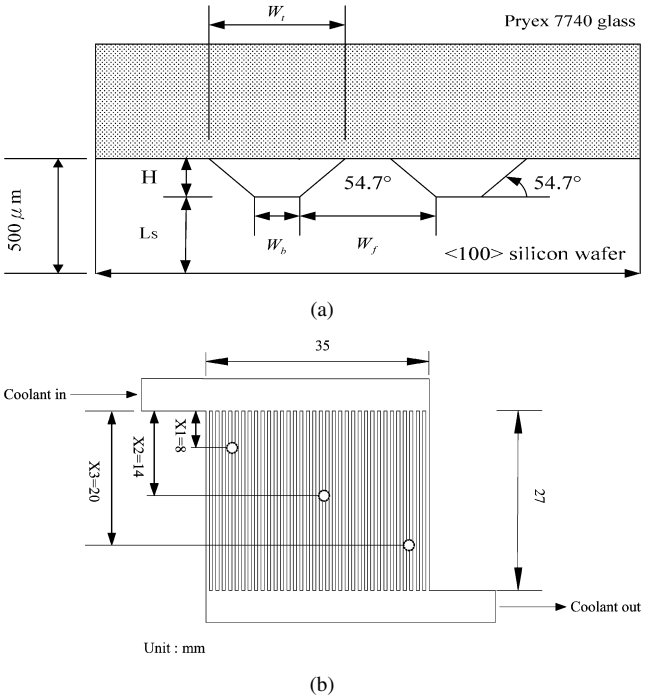

Fig. 2. (a) Microchannel geometry. (b) Microchannel heat sink configuration and base plate temperature measurement locations.

The silicon microchannel heat sink shown in Fig. 2 was then installed into a Teflon cavity along with thermal insulating layer and film heater to form the test module as shown in Fig. 3. The film heater coated with an electrical insulating layer was used to simulate the heat flux generated by the electronic chip. The heater was energized by a DC power supply which could be regulated in the ranges of 0–30 V and 0–3 A. Three T-type thermocouples of 0.1 mm in diameter are attached at X1, X2 and X3 and sandwiched in between the heater and MCHS base plate. A thermal insulating layer was placed at the bottom of the Teflon cavity to reduce the heat loss from the heater. These structures were secured to the Teflon base by applying clamps around the Teflon base rims to ensure good contact and tightness between MCHS base plate, thermocouples and heater.

The data acquisition system consisted of a computer, 16-bit, 16-channel PCMCIA A/D card, and signal conditioning circuitry. The system was controlled using Labview programs.

3.2. Experimental device calibrations and experimental procedures

The experiment starts from turning on the pump and heater for specific flow rate and heating power. All of the pressure and

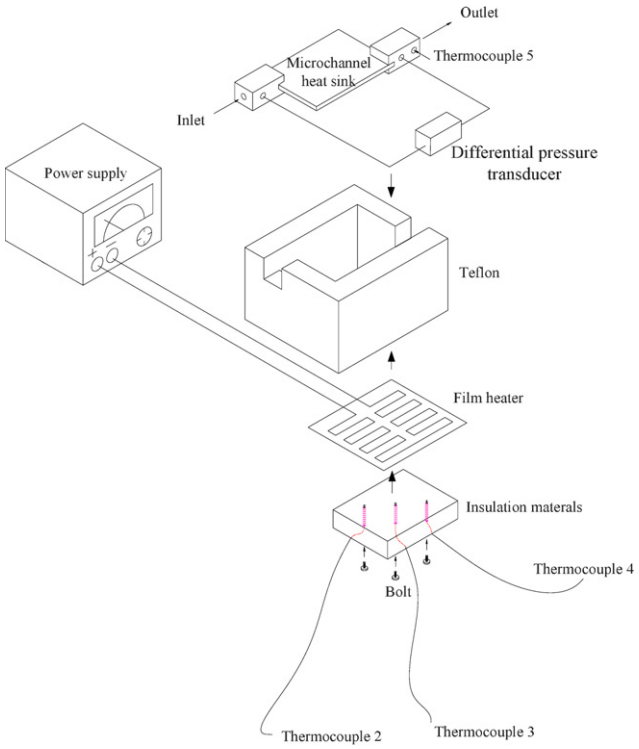

Fig. 3. Microchannel heat sink test module assembly.

temperature signals were recorded in the data acquisition system for analyses after the steady state was reached. Because a nanofluid was used as working fluid, the pump flow rate might be sensitive to the fluid viscosity and calibration was needed. As mentioned above, a flow meter with accuracy of ±0.5% was connected at the entrance of the MCHS test module to check the flow rate in the flow loop. The differential pressure transducer was factory calibrated with an uncertainty of ±0.2% at the nominal value 50 kPa. All the thermocouples were calibrated in a thermostat water bath and the accuracy was found to be within 0.2 K. The input voltage and current to the heater were controlled by a power supply with accuracies of 0.5%. In order to exclude the effect of particle deposition on the temperature measurement, a brand new MCHS was employed when the working fluid was changed.

As stated above, the MCHS was installed in a Teflon cavity which has very low thermal conductivity. An insulation layer was also coated around the cavity for further reducing heat loss from the Teflon cavity. The only possible heat loss occurs at the top surface of the MCHS which is made of glass. The heat transfer mechanisms at this surface are via radiation and natural convection. The heat loss due to these two mechanisms is expected to be low because of low surface temperature and heat transfer coefficient [22].

3.3. Working fluid

In this study, the working fluids were deionized water and nanofluid. The results obtained from pure water are used as comparison basis. The nanofluid used in this study was a CuO–H_2O mixture obtained using the arc-submerged nanoparticle synthesis system [23–25]. In this method, a pure copper rod is submerged in the DI water contained in a vacuum chamber. The copper rod is heated and melted by high energetic electric arc. At the same time, the DI water surrounding the melted rod is also vaporized and cause the vaporized metal to move away from the copper rod. The vaporized metal undergoes nucleation, growth, condensation and finally turning into nanoparticles dispersed in the DI water. The low-temperature DI water in the chamber provides the condensation environment for the production of nanoparticles. No dispersion agent was added to prevent the particles from agglomerating in this synthesis process. Since the particles are directly dispersed in the base fluid, the volume fraction cannot be computed using the amount of nanoparticle added [15]. The method of measuring particle volume fraction is to employ the UV-visible spectrometer (UVmini-1240, Shimadzu, Japan). The wavelength accuracy of this device is ±1.0 nm. The particle volume fraction can be evaluated from the ratio of light absorbed by the suspended particle to the light that passing through the bulk fluid. In this study, nanofluid with three different particle volume fractions as tabulated in Table 1 were used in the test. The relevant thermophysical properties of these fluids are also listed in Table 1. The thermal conductivity of nanofluid was measured using a KD2 thermal property meter which is based on the transient hot wire method [26]. The other properties listed in Table 1 were computed using the formula given in Eqs. (2) and (3). Properties of CuO particle were taken from the measurements reported by Chen et al. [27]. Fig. 4 shows the fabricated nanofluids and a TEM image of dispersed CuO nanoparticles in water with volume fraction of 0.294%. The CuO–H_2O nanofluid has brown

Table 1
Thermophyscial properties of CuO–H_2O nanofluid

Particle volume fraction, ϕ [%]	Thermal conductivity, k_{nf}	Viscosity, μ_{nf}	Thermal capacity, $(\rho C_p)_{nf}$
0.204	0.61	0.0008946	4165203
0.256	0.62	0.0008956	4163301
0.294	0.63	0.0008966	4161482
0.4	0.65	0.0008990	4157100

Note. (1) Properties of water are evaluated at 20 °C: $C_P = 4182$ (J kg^{-1} K^{-1}), $\rho = 998$ kg^{-1} m^{-3}, and $\mu = 0.00089$ N S m^{-2}. (2) Properties of CuO are evaluated at 20 °C: $C_P = 6.27$ (J kg^{-1} K^{-1}), $\rho = 6320$ kg m^{-3} [27].

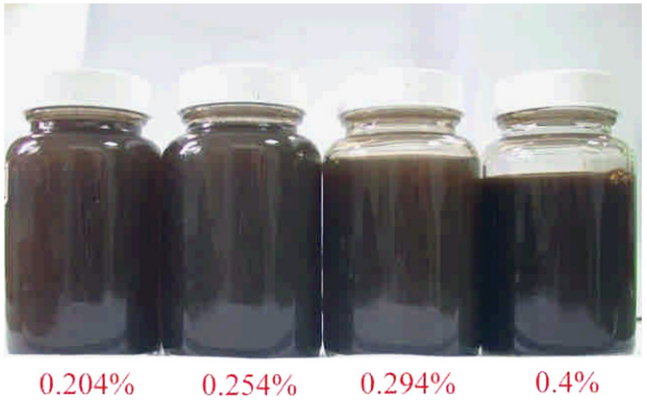

(a)

(b)

Fig. 4. (a) CuO–H_2O nanofluids before used as coolants, $\phi = 0.294\%$. (b) TEM image of suspended nanoparticles in CuO–H_2O nanofluid shown in (a).

color and increases its darkness with the increase of particle volume fraction. In the TEM image, it is seen that the CuO particle has needle shape and distributes uniformly in the water. The particle sizes are quite uniform with averaged length and width are approximately 80 nm and 20 nm, respectively.

In most of the studies in the past, surfactants and/or dispersants were generally used to enhance the steric barriers between nanoparticles, therefore to stabilize the nanofluid. However, cares must be taken as these surfactants/dispersants could have significant influence on the flow and heat transfer. Moreover, these surfactants/dispersants may fail when the bulk temperature is increased. In this study, no dispersant was added in the nanofluid, it is one of our goals to investigate the performance and limitation of using nanofluid as working fluid.

4. Results and discussion

4.1. Energy absorbed by the working fluids

We first examined the amount of energy that could be absorbed by the working fluid to verify the $Q_{nf} > Q_f$ assumption. As mentioned in the theoretical prediction, the flow rate and MCHS inlet temperature for both nanofluid- and water-cooled MCHS should remain the same. In this study, the flow rates were chosen at $\dot{V}_{nf} = \dot{V}_f = \dot{V} = 10, 15$ and 20 mL min^{-1} and the MCHS inlet temperature was fixed at 20 °C. The heating power from the heater was fixed at 25.3 W. The measured energies absorbed by the working fluids shown in Fig. 5(a) were calculated using Eqs. (4) and (5). The measured temperature differences between MCHS inlet and outlet were shown in Fig. 5(b). For the $\dot{V} = 10$ mL min^{-1} case, only part of the input heating power could be absorbed by the working fluid. The measured data indicated that amount of energy absorbed by the nanofluid was greater than that absorbed by the water. The amount of energy absorbed was found to increase with the increase in particle volume fraction. Since the only difference between the nanofluid and water was the presence of nanoparticles, it is believed that nanoparticles can contribute to additional heat absorption capability. However, as flow rates increases to 15 and 20 mL min^{-1}, both nanofluid and water can nearly absorb all the input heating power. At these high flow rates, the heat transport is dominated by the mass flow rate and the presence of nanoparticles did not contribute to extra energy absorption. As indicated in Fig. 5(b), large temperature difference between MCHS inlet and outlet was obtained when the flow rate was low, even when only part of the heating power was absorbed by the working fluid.

4.2. Wall temperatures along the nanofluid-cooled MCHS base plate

To verify the second assumption of theoretical prediction, that is, $h_{nf}(x) > h_f(x)$, temperatures at three MCHS base plate locations are measured and the results are shown in Figs. 6, 7 and 8 for $\dot{V} = 10, 15$, and 20 mL min^{-1}. Because the silicon has high thermal conductivity, the measured temperatures on the MCHS base plate can be regarded as the microchannel

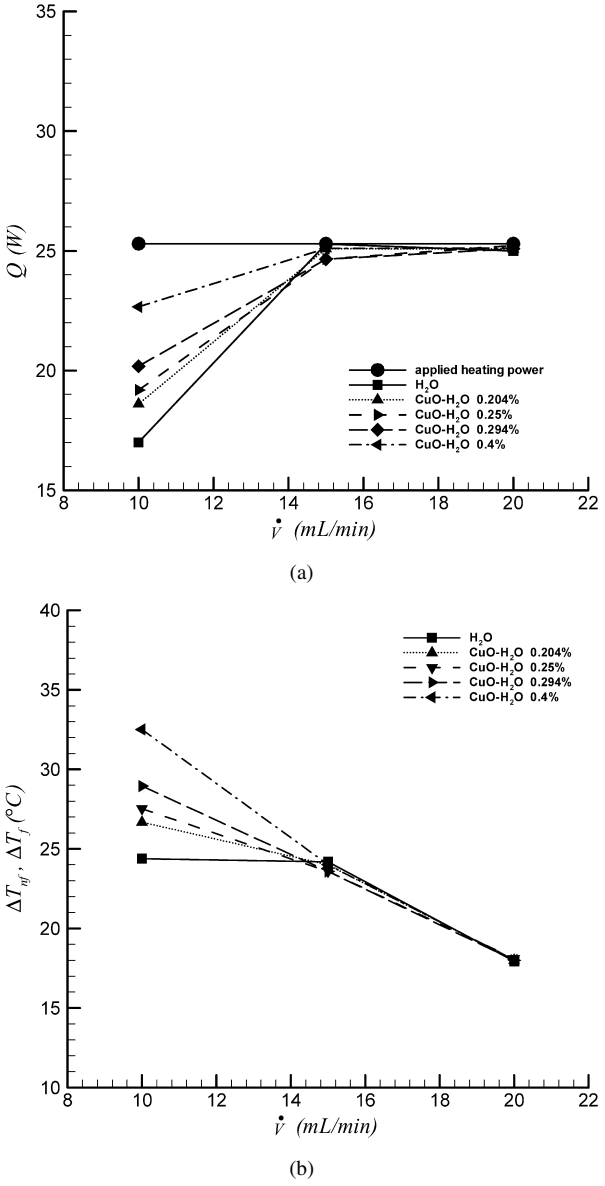

Fig. 5. (a) Energy absorbed by the working fluids flowing through the MCHS. (b) Temperature difference between inlet and outlet as nanofluid flowing through the MCHS.

inner wall temperatures. In the $\dot{V} = 10$ mL min^{-1} case, the temperature variation range is higher as compared with those of $\dot{V} = 15$ and 20 mL min^{-1} cases because part of heating power is stored in the MCHS. The measured MCHS wall temperatures as shown in Fig. 6 agreed with the theoretical prediction ($(T_{snf}(x) < T_{sf}(x))$. For the particle volume fraction range studied, it was found that MCHS wall temperatures decrease with the increase in particle volume fraction. This implies that heat transfer could be enhanced further using nanofluid with higher particle concentration. This result agreed with the results reported for the nanofluid heat transfer in macroscale dimensions [14,15]. As flow rate increases to 15 and 20 mL min^{-1}, however, the measured MCHS wall temperature did not completely agree with the theoretical predictions. Using the optical microscope to examine the MCHS after the test finished, it was found that serious particle deposition occurs inside the channels as

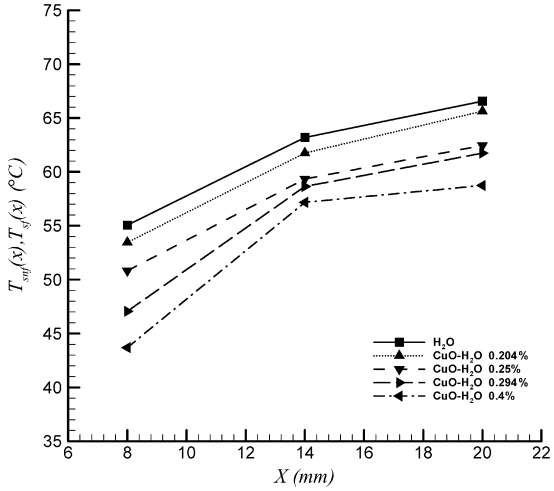

Fig. 6. MCHS base plate temperature variation, $\dot{V} = 10\ \mathrm{mL\,min^{-1}}$.

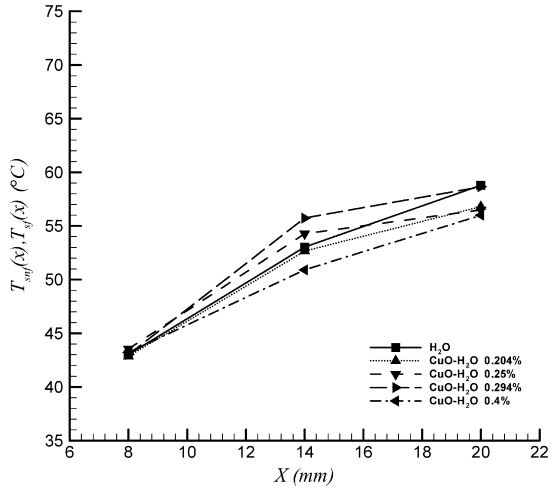

Fig. 7. MCHS base plate temperature variation, $\dot{V} = 15\ \mathrm{mL\,min^{-1}}$.

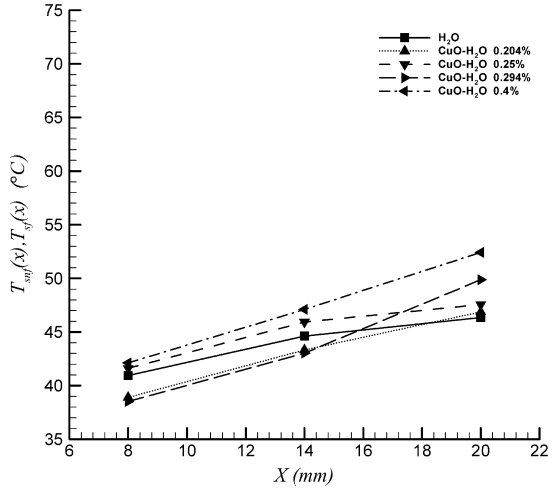

Fig. 8. MCHS base plate temperature variation, $\dot{V} = 20\ \mathrm{mL\,min^{-1}}$.

well as the inlet and outlet ports. Typical particle deposition situations are shown in Fig. 9 for $\dot{V} = 20\ \mathrm{mL\,min^{-1}}$ case. For the water-cooled case, no particle deposition was found and the

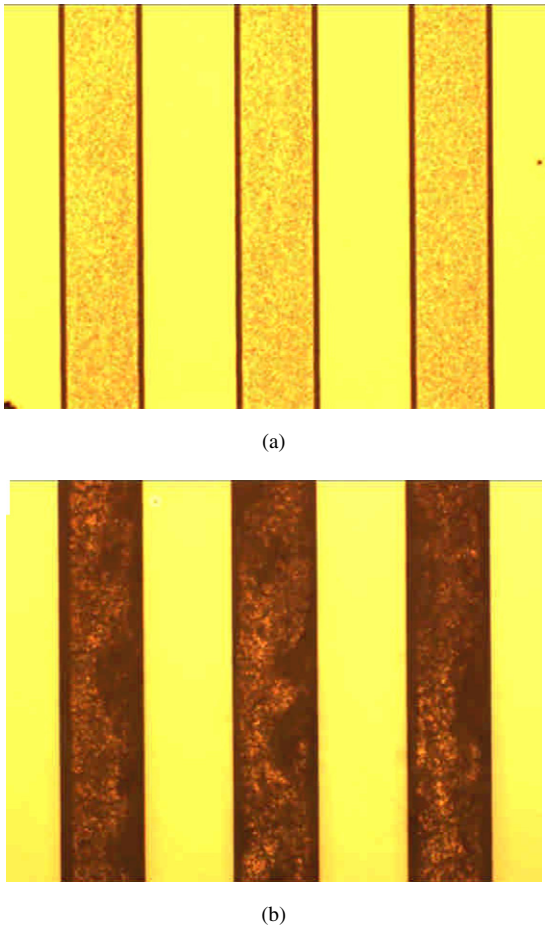

(a)

(b)

Fig. 9. Optical microscopic images of particle deposition in MCHS. (a) Water-cooled MCHS. (b) Nanofluid-cooled MCHS.

channel surface was clean. However, the microchannel surface seemed to be coated with a layer of particles in the nanofluid-cooled microchannels. In the macroscale dimensions, it was reported that the degree of heat transfer enhancement increased with the increase in particle volume fraction [14,15]. However, the particle volume fraction was expected to decrease if particle deposition onto the channel wall occurred. Particle deposition rate prediction and consequently the particle volume fraction are difficult to obtain because a complicated particle deposition process was involved, especially for nonspherical particles. It is believed that these reasons contribute to the disagreements between theoretically predicted and experimentally measured MCHS wall temperatures shown in Figs. 7 and 8.

Reason for particle deposition onto the walls can be found by examining the nanoparticle structure after the nanofluid has been used as the coolant. In Fig. 10, the used nanofluid and its TEM image are shown with particle volume fraction of 0.294% for the $\dot{V} = 20\ \mathrm{mL\,min^{-1}}$ test. By comparing Fig. 4 and Fig. 10, the used nanofluid was darker in color. In the TEM image, it is seen that nanoparticles agglomerated and connected together to form large scale particle clusters. These large scale particle clusters would eventually deposit onto the wall under the gravitational effect and affect the MCHS wall temperature measurements.

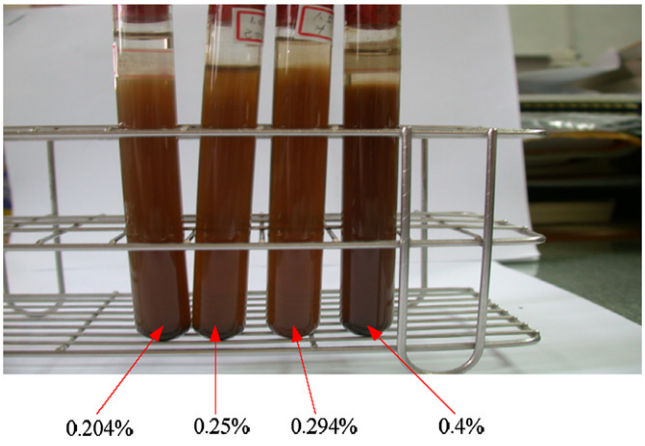

(a)

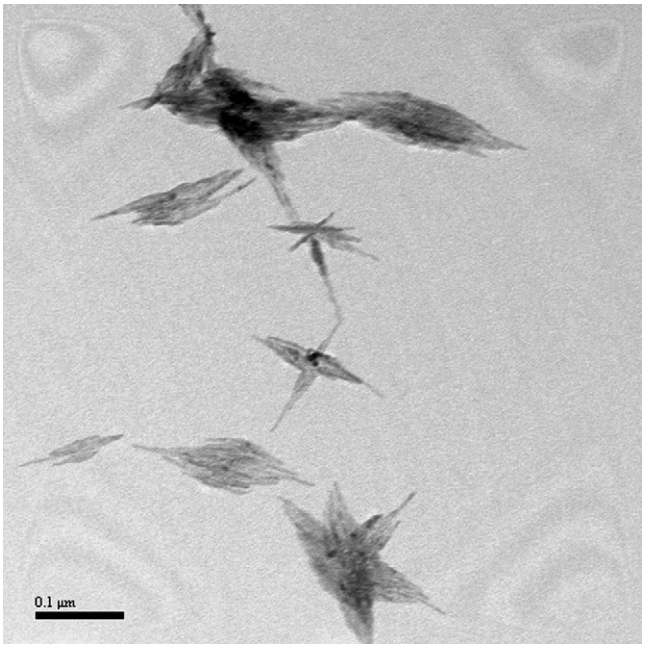

(b)

Fig. 10. (a) CuO–H_2O nanofluids after used as coolants, $\phi = 0.294\%$ and $\dot{V} = 20\ \mathrm{mL\,min^{-1}}$. (b) TEM image of CuO–$H_2O$ nanofluid shown in (a).

As shown in Fig. 5(b), the bulk temperature of nanofluid is higher when the volume flow rate is low. For such case, the measured MCHS wall temperature variation agreed with the theoretical prediction. This implies that particle deposition can be prevented when the nanofluid temperature is increased. Particle deposition is a complicated process involving particle-particle and particle-wall interactions. These interactions are related to the particle shape, particle size, electrochemical and thermophysical properties of bulk fluid, particle, and wall and bulk fluid temperature [28]. In addition, forces acting on particle are also important in the particle deposition process. When a temperature gradient is present in a flow field, the particle experiences thermophoretic force in addition to drag and lift forces. The resultant thermophoretic force has a direction pointing to the low-temperature region in the flow field [29,30]. In our study, it was observed that microchannel wall temperature is higher when fluid flow rate is lower. Therefore, stronger thermophoretic force may act on the agglomerated particle or unagglomerated particles and keeping them away from the wall. That is, less particle deposition could be expected at higher temperature.

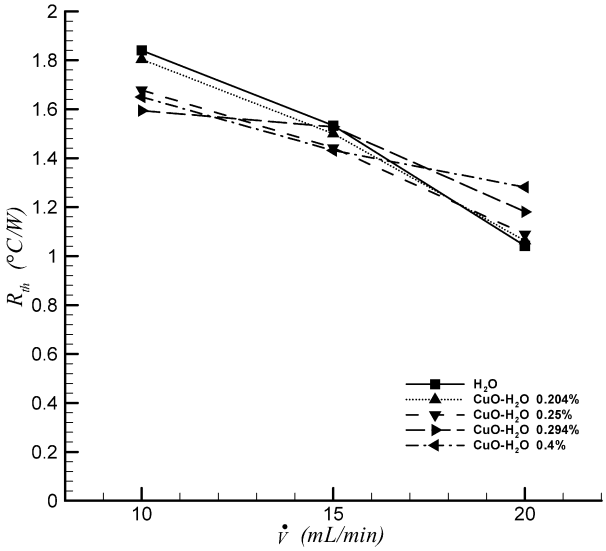

Fig. 11. Thermal resistance as function of flow rate for both nanofluid- and water-cooled MCHS.

In most of the studies in the past, there is no particle deposition on the channel or tube wall has been reported. This may be due to the difficulty in performing the flow visualization since the opaque metal tubes or channels were generally used in the experiments. In our opinion, particle agglomeration cannot be prevented even the surfactants were added, especially when nanofluid is heated. The larger particle would be formed due to particle agglomeration and consequently the particle deposition onto the wall occurs. The surfactants might delay the particle agglomeration but eventually particle agglomeration occurs and deposit on the wall. The surfactant may be considered as a substance delaying the particle deposition in the heat transfer applications. In this study, one of the goals is to address how the particle deposition affects the heat transfer characteristics. It was found that particle deposition plays an important role in the heat transfer measurements.

4.3. MCHS thermal resistance

Although the measured MCHS wall temperature did not completely agree with the theoretical prediction, the MCHS thermal resistances were calculated in this study since it is usually used as an indication of heat sink performance. Because the wall temperature measured at X3 is close to the microchannel exit, the temperatures measured at this location were treated as the maximum microchannel wall temperatures. The computed thermal resistances for both nanofluid- and water-cooled MCHS using Eq. (12) are shown in Fig. 11. Thermal resistance reduces as the flow rate increases, which agreed with the performance of conventional MCHS [4]. The nanofluid-cooled MCHS had lower thermal resistance for flow rates of 10 and 15 $\mathrm{mL\,min^{-1}}$. When the flow rate was increased to 20 $\mathrm{mL\,min^{-1}}$, the performance of the nanofluid-cooled MCHS

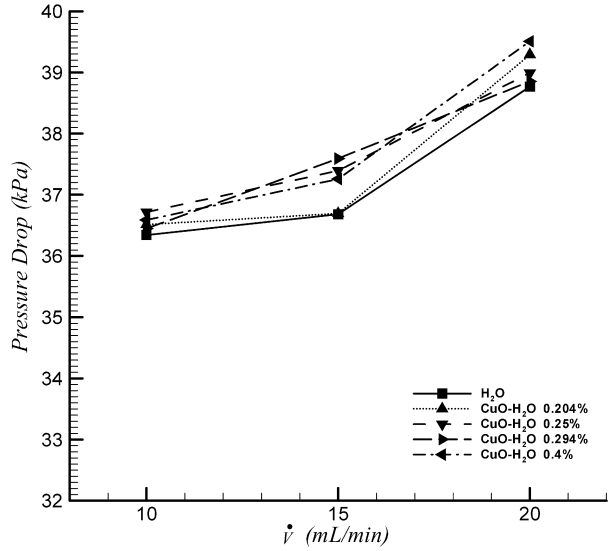

Fig. 12. Pressure drop across the MCHS as function of flow rate for both nanofluid- and water-cooled MCHS.

was worse than that of the water-cooled MCHS because of serious particle deposition.

4.4. MCHS pressure drop

Another important parameter in the MCHS operation is the pressure drop. The pressure drop is related to the pumping power required for driving the fluid flowing through the MCHS. The measured results for the pressure drops of both nanofluid-cooled and pure water cooled-MCHS are shown in Fig. 12. Compared with the pure water cooled case, slightly larger pressure drops for the nanofluid-cooled MCHS were found. Since the viscosity of nanofluid is larger than the pure fluid as indicated in Eq. (2), larger pressure drop is expected in the nanofluid-cooled MCHS. The other reason that contributes to increase in pressure drop is due to the particle deposition that increasing the wall roughness. Considering the enhancement of overall heat transfer performance can be achieved, slightly increase in pressure drop can be considered one of the benefits of using a nanofluid in MCHS operations.

5. Conclusion

The performances of MCHS using nanofluids as the coolants were studied. We first carried out a simple theoretical prediction and followed by experimental verifications. The following conclusions can be made according to our study:

(1) The theoretical prediction indicated that the nanofluid-cooled MCHS could absorb more heat and attain lower wall temperatures than MCHS using pure fluid provided that the heat transfer could be enhanced by the nanofluid flow.
(2) The experimental results indicated that the nanofluid flow did absorb more energy as compared with the pure fluid flow due to the presence of nanoparticles. However, nanoparticles contribute no extra heat absorption when the flow rate is high.
(3) For a low flow rate, the measured MCHS wall temperature variation agreed with the theoretical predictions. In high flow rates cases, the measured MCHS wall temperatures did not completely agree with the theoretical prediction due to particle agglomeration and deposition. It was also found that particle agglomeration could be prevented when the nanofluid has a higher bulk temperature.
(4) Although the nanofluid has higher viscosity, only a slight increase in the pressure drop across the MCHS was found compared with the pure fluid-cooled MCHS.

References

[1] D.B. Tuckerman, R.F. Pease, High-performance heat sinking for VLSI, IEEE Electronic Devices Letters, EDL 2 (1981) 126–129.
[2] H.Y. Wu, P. Cheng, An experimental study of convective heat transfer in silicon microchannels with different surface conditions, Int. J. Mass Heat Transfer 46 (2003) 2547–2556.
[3] W. Qu, I. Mudawar, Experimental and numerical study of pressure drop and heat transfer in a single-phase micro-channel heat sink, Int. J. Heat Mass Transfer 45 (2002) 2549–2565.
[4] R.W. Knight, D.J. Hall, J.S. Goodling, R.C. Jaeger, Heat sink optimization with application to microchannels, IEEE Transactions on Components, Hybrids, and Manufacturing Technology 15 (1992) 832–842.
[5] A. Horvat, I. Catton, Numerical technique for modeling conjugate heat transfer in an electronic device heat sink, Int. J. Heat Mass Transfer 46 (2003) 2155–2168.
[6] K.V. Liu, S.U.S. Choi, K.E. Kasza, Measurements of pressure drop and heat transfer in turbulent pipe flows of particulate slurries, Report, Argonne National Laboratory, 1988, ANL-88-15.
[7] R.L. Webb, Principles of Enhanced Heat Transfer, John Wiley & Sons, New York, 1993.
[8] X. Wang, X. Xu, S.U.S. Choi, Thermal conductivity of nanoparticle-fluid mixture, J. Thermophys. Heat Transfer 13 (1999) 474–480.
[9] S. Lee, S.U.S. Choi, S. Li, J.A. Eastman, Measuring thermal conductivity of fluids containing oxide nanoparticles, J. Heat Transfer 121 (1999) 280–289.
[10] B.X. Wang, L.P. Zhou, X.F. Peng, A fractal model for predicting the effective thermal conductivity of liquid with suspension of nanoparticles, Int. J. Heat Mass Transfer 46 (2003) 2665–2672.
[11] J. Koo, C. Kleinstreuer, A new thermal conductivity model for nanofluids, J. Nanoparticle Research 6 (2004) 577–588.
[12] Y. Xuan, W. Roetzel, Conceptions for heat transfer correlation of nanofluids, Int. J. Heat Mass Transfer 43 (2000) 3701–3707.
[13] Q. Li, Y. Xuan, Convective heat transfer and flow characteristics of Cu–water nanofluid, Science in China, Series E 45 (2002) 408–416.
[14] Y. Xuan, Q. Li, Investigation on convective heat transfer and flow features of nanofluids, ASME J. Heat Transfer 125 (2003) 151–155.
[15] B.C. Pak, Y.L. Cho, Hydrodynamic and heat transfer study of dispersed fluids with submicron metallic oxide particles, Exp. Heat Transfer 11 (1998) 151–170.
[16] Y. Yang, Z. Zhang, E.A. Grulke, W.B. Anderson, Heat transfer properties of nanoparticle-influid dispersions (nanofluids) in laminar flow, Int. J. Heat Mass Transfer 48 (2005) 1107–1116.
[17] J. Koo, C. Kleinstreuer, Laminar nanofluid flow in microheat-sinks, Int. J. Heat Mass Transfer 48 (2005) 2652–2661.
[18] R. Chein, G. Hunag, Analysis of microchannel heat sink performance using nanofluids, Applied Thermal Engineering 25 (2005) 3104–3114.
[19] R.L. Hamilton, O.K. Crosser, Thermal conductivity of heterogeneous two-component systems, I and CE Fundamentals 1 (1962) 187–191.
[20] A.R.A. Khaled, K. Vafai, Heat transfer enhancement through control of thermal dispersion effects, Int. J. Heat Mass Transfer 48 (2005) 2172–2185.
[21] H.C. Brinkman, The viscosity of concentrated suspension and solutions, J. Chemistry Physics 20 (1952) 571–581.

[22] I. Tiselj, G. Hetsroni, B. Mavko, A. Mosyak, E. Pogrebnyak, Z. Segal, Effect of axial conduction on the heat transfer in microchannels, Int. J. Heat Mass Transfer 47 (2004) 2551–2565.
[23] C.H. Lo, T.T. Tsung, L.C. Chen, C.H. Su, H.M. Lin, Fabrication of copper oxide nanofluid using submerged arc nanoparticle synthesis system (SANSS), J. Nanoparticle Res. 7 (2005) 313–320.
[24] H. Chang, C.S. Jwo, C.H. Lo, T.T. Tsung, M.J. Kao, H.M. Lin, Rheology of CuO nanoparticle suspension prepared by ASNSS, Rev. Adv. Mater. Sci. 10 (2005) 128–132.
[25] C.H. Lo, T.T. Tsung, Low-than-room temperature effect on the stability of CuO nanofluid, Rev. Adv. Mater. Sci. 10 (2005) 64–68.
[26] W.A. Wakeham, A. Nagashime, J.V. Sengers, Measurement of Transport Properties of Fluids, Blackwell Scientific, Oxford, UK, 1991.
[27] Y.Y. Chen, Y.D. Yao, B.T. Lin, C.T. Suo, S.G. Shyu, H.M. Lin, Specific heat of fine copper particles, Nanostructured Materials 6 (1995) 597–600.
[28] J. Israelachvili, Intermolecular and Surface Forces, Academic Press, New York, 1992.
[29] G.S. McNab, A. Meisen, Thermophoresis in liquid, J. Colloid Interface Sci. 44 (1973) 339–346.
[30] P. Adomeit, U. Renz, Deposition of fine particles from a turbulent liquid flow: experiments and numerical predictions, Int. J. Heat Mass Transfer 51 (1996) 3491–3503.